

In-plane optical anisotropy of two-dimensional VOCl single crystal with weak interlayer interaction

Ruijie Wang(王瑞洁), Qilong Cui(崔其龙), Wen Zhu(朱文), Yijie Niu(牛艺杰), Zhanfeng Liu(刘站锋), Lei Zhang(张雷), Xiaojun Wu(武晓君), Shuangming Chen(陈双明), and Li Song(宋礼)

Citation: Chin. Phys. B, 2022, 31 (**9**): 096802. DOI: 10.1088/1674-1056/ac7555
Journal homepage: http://cpb.iphy.ac.cn; http://iopscience.iop.org/cpb

What follows is a list of articles you may be interested in

Ohmic and Schottky contacts of hydrogenated and oxygenated boron-doped single-crystal diamond with hill-like polycrystalline grains

Jing-Cheng Wang(王旌丞), Hao Chen(陈浩), Lin-Feng Wan(万琳丰), Cao-Yuan Mu(牟草源), Yao-Feng Liu(刘尧峰), Shao-Heng Cheng(成绍恒), Qi-Liang Wang(王启亮), Liu-An Li(李柳暗), and Hong-Dong Li(李红东)

Chin. Phys. B, 2021, 30 (**9**): 096803. DOI: 10.1088/1674-1056/ac032b

Selective linear etching of monolayer black phosphorus using electron beams

Yuhao Pan(潘宇浩), Bao Lei(雷宝), Jingsi Qiao(乔婧思), Zhixin Hu(胡智鑫), Wu Zhou(周武), Wei Ji(季威)

Chin. Phys. B, 2020, 29 (**8**): 086801. DOI: 10.1088/1674-1056/ab9438

Epitaxial fabrication of two-dimensional $TiTe_2$ monolayer on Au(111) substrate with Te as buffer layer

Zhipeng Song(宋志朋), Bao Lei(雷宝), Yun Cao(曹云), Jing Qi(戚竞), Hao Peng(彭浩), Qin Wang(汪琴), Li Huang(黄立), Hongliang Lu(路红亮), Xiao Lin(林晓), Ye-Liang Wang(王业亮), Shixuan Du(杜世萱), Hong-Jun Gao(高鸿钧)

Chin. Phys. B, 2019, 28 (**5**): 056801. DOI: 10.1088/1674-1056/28/5/056801

Photodetecting and light-emitting devices based on two-dimensional materials

Yuanfang Yu(于远方), Feng Miao(缪峰), Jun He(何军), Zhenhua Ni(倪振华)

Chin. Phys. B, 2017, 26 (**3**): 036801. DOI: 10.1088/1674-1056/26/3/036801

In-plane anisotropy in two-dimensional electron gas at $LaAlO_3/SrTiO_3$(110) interface

Sheng-Chun Shen(沈胜春), Yan-Peng Hong(洪彦鹏), Cheng-Jian Li(厉承剑), Hong-Xia Xue(薛红霞), Xin-Xin Wang(王欣欣), Jia-Cai Nie(聂家财)

Chin. Phys. B, 2016, 25 (**7**): 076802. DOI: 10.1088/1674-1056/25/7/076802

In-plane optical anisotropy of two-dimensional VOCl single crystal with weak interlayer interaction

Ruijie Wang(王瑞洁)[1,†], Qilong Cui(崔其龙)[1,†], Wen Zhu(朱文)[1,2,†], Yijie Niu(牛艺杰)[3], Zhanfeng Liu(刘站锋)[1], Lei Zhang(张雷)[4], Xiaojun Wu(武晓君)[3], Shuangming Chen(陈双明)[1,‡], and Li Song(宋礼)[1]

[1] *National Synchrotron Radiation Laboratory, University of Science and Technology of China (USTC), Hefei* 230029, *China*
[2] *School of Mechanical Engineering, Shanghai Jiao Tong University, Shanghai* 200240, *China*
[3] *Department of Materials Sciences and Engineering, School of Chemistry and Materials Sciences, University of Science and Technology of China, Hefei* 230026, *China*
[4] *School of Materials Science and Physics, China University of Mining and Technology, Xuzhou* 221116, *China*

(Received 25 April 2022; revised manuscript received 30 May 2022; accepted manuscript online 2 June 2022)

Transition-metal oxyhalides MOX (M = Fe, Cr, V; O = oxygen, X = F, Cl, Br, I), an emerging type of two-dimensional (2D) van der Waals materials, have been both theoretically and experimentally demonstrated to possess unique electronic and magnetic properties. However, the intrinsic in-plane anisotropic properties of 2D VOCl still lacks in-depth research, especially optical anisotropy. Herein, a systematic Raman spectroscopic study is performed on VOCl single-crystal with different incident laser polarization at various temperatures. The polarized-dependent Raman scattering spectra reveal that the A_g mode of VOCl show a 2-lobed shape in parallel polarization configuration while a 4-lobed shape in vertical configuration. In addition, the temperature-dependent and thickness-dependent Raman scattering spectra confirm a relatively weak van der Waals interaction between each layers among VOCl single crystal. These findings might provide better understanding on the in-plane anisotropic phenomenon in VOCl layers, thus will accelate further application of 2D single crystals for nanoscale angle-dependent optoelectronics.

Keywords: two-dimensional (2D) materials, in-plane anisotropy, Raman spectra

PACS: 68.65.–k, 78.67.–n, 78.30.–j **DOI:** 10.1088/1674-1056/ac7555

1. Introduction

Two-dimensional (2D) materials, such as black phosphorus,[1–3] tellurium,[4] and transition metal dichalcogenide (TMDs),[5–15] show unique in-plane electrical, magnetic, optical, and thermal anisotropy due to their anisotropy of crystal structure. These characteristics endow 2D materials great potential in a diverse angle-dependent optoelectronic application.[3,16,17] Based on the above views, the fundamental physical properties, such as polarization-dependent behavior and phonon modes, are critical for the design of high-performance devices based on 2D materials with in-plane anisotropic properties.

As one of the 2D transition-metal oxyhalides (M = Fe, Cr, V; O = oxygen, X = F, Cl, Br, I), VOCl has been widely studied for its physical properties and applications. Among them, theoretical calculations predicted that it is a multiorbital Mott-insulator, and the bandgap is about 2 eV with high resistivity.[18–20] Recently, VOCl single-crystal have been demonstrated possess high dielectric constant[20] and strong spin-phonon coupling.[21] Besides, research on similar materials has also been carried out widely. For example, CrOCl/CrOBr monolayer have been identified as intrinsic ferromagnetic semiconductors with Curie temperatures of up to 160 K and 129 K, respectively.[22] Ultrathin ytterbium oxychloride (YbOCl) single crystals are successfully synthesized via chemical vapor deposition (CVD) method.[23] However, the intrinsic in-plane anisotropic properties of 2D VOCl still lacks in-depth research.

Raman spectroscopy is a non-destructive method to investigate the anisotropy properties of 2D materials because it can provide structural and electronic information of characterized 2D materials with high spectral and spatial resolution together.[24–26] Using angle-resolved Raman spectroscopy, the polarization-dependent behavior of 2D materials can be exploited.[27] And temperature-dependent Raman spectroscopy can show the temperature effect of the phonon mode and enables us to further understand the atomic structure, valence bond, electrical, and thermal properties of the material being studied.[28,29] Furthermore the thickness-dependent Raman spectra can also reflect influence of 2D materials interlayer force on phonon and photon vibrational modes.

Herein, we synthesized the single crystal of VOCl by the chemical vapor transport (CVT) method successfully, the polarization-dependent behavior of VOCl is detected by using polarized Raman scattering on the (001) crystal plane, then the strong in-plane vibrational anisotropy of 2D VOCl

[†]These authors contributed equally to this work.
[‡]Corresponding author. E-mail: csmp@ustc.edu.cn

© 2022 Chinese Physical Society and IOP Publishing Ltd

is demonstrated. The Raman peaks are shown in the range of 100 cm^{-1}–500 cm^{-1}, and nuclear site group theory is used to distinguish the different Raman modes correspond to peaks. The temperature-dependent Raman experiment is performed to study the lattice vibrational behavior and showed the phonon modes change at 150 K. The corresponding Raman spectra of VOCl flakes with different thickness indicate the weak interlayer van der Waal interaction in VOCl crystals.[30] This work could provide useful information for the convenience of 2D materials in the field research of electronics and optics.

2. Experiment details

2.1. Synthesis of VOCl

The VOCl single crystal was prepared by the CVT method. Firstly, the V_2O_3 powders were synthesized by annealing the V_2O_5 (99%, Aldrich) in Ar/H2 (10%) atmosphere with a flow rate of 100 sccm, the furnace was heated to 600 °C in 60 min, and kept at this temperature for 30 min, then the temperature rose to 900 °C in 30 min and hold for 2 hours, the furnace was cooled down naturally. Secondly, in the glove box, the V_2O_3 and VCl_3 (99%, Aldrich) were weighed in a stoichiometric ratio and placed in a quartz glass tube, then the tube was taken out, evacuated to 6×10^{-3} Pa, and sealed by propane and oxygen gas. Thirdly, this tube was put in a two-zone furnace with a temperature gradient of 850 °C–750 °C and held for 5 days. After natural cooling, single-crystal samples can be obtained.

2.2. Transfer and characterizations

The VOCl crystal was mechanically exfoliated by scotch tape and transferred to 300-nm SiO_2/Si substrate with PDMS. The size, morphology, and thickness of as-grown VOCl samples were characterized by OM (Olympus BX53-P) and AFM (Bruker Dimension Icon). Raman and PL spectra were obtained from a confocal microscope Raman spectrometer (HORIBA LabRAM HR-800, 532-nm excitation laser with 1 mW). The high-resolution TEM (HRTEM) and corresponding SAED analyses were performed on a JEOL (JEMARF200F TEM). The x-ray absorption fine structure (XAFS) spectra were collected in the Beijing Synchrotron Radiation Facility (1W1B, BSRF) to detect the V *K*-edges. The x-ray was monochromatized by an Si(111) monochromator.

3. Results and discussion

3.1. Characterization of synthesized VOCl

For atomic model, VOCl single crystal has a symmetry of D_{2h}^{12} (*Pmmn*) point group. Each molecular layer contains two layers of chlorine atoms sandwiched between a V–O bimolecular layer, and the molecular layers are coupled by van der Waals forces (Fig. 1(a)). The powder x-ray pattern of the VOCl crystals is shown in Fig. 1(b). Four peaks including (001) peak at 11.44°, (003) peak at 34.08°, (004) peak at 45.9°, and (005) peak at 58.3° are confirmed, indicating the preferential growth orientation of VOCl is (001) plane.

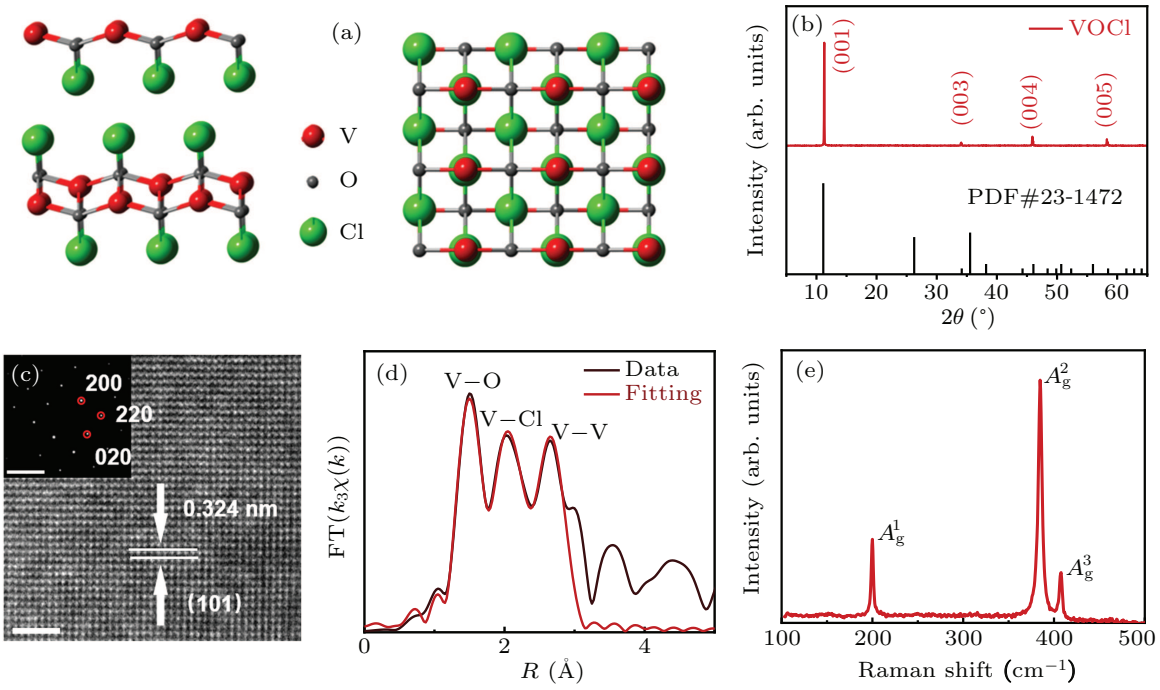


Fig. 1. Synthesis and characterization of VOCl single crystals. (a) The crystal structure of VOCl under side and top views. (b) Powder x-ray pattern of the VOCl crystals. (c) The TEM image of VOCl crystals, scale bar: 2 nm. And the selective area electron diffraction of VOCl, scale bar: 5 1/nm. (d) The corresponding Fourier transforms FT($k^3\chi(k)$) and the first shell fitting of Fourier transform of XAFS spectra (V–V, V–O, and V–V) for VOCl. (e) Raman spectra of VOCl at 93 K.

Figure 1(c) show the transmission electron microscopy (TEM) image and the selective area electron diffraction (SAED) spots of VOCl, which reveals the arrangement of atoms on the (101)-basal plane, the lattice spacing of the crystal planes of (101) can be measured at 0.324 nm. Meanwhile, the SAED spots reflects the high crystallinity of VOCl. Besides, the (200), (220), and (020) planes are confirmed from the [001] zone axis.

In addition, x-ray absorption fine structure (XAFS) is also used to determine the crystal structure of VOCl (see Section 2 for XAFS experimental parameters). The XAFS results of VOCl, V_2O_3 and VO_2 single crystals (see Fig. S1) show that, with the V_2O_3 and VO_2 as references, the absorption edge of V shifts to lower energies, indicating the V valence state is about +3. The coincidence of its fourier transform spectra of extended XAFS (V–O, V–Cl, and V–V) and first shell fitting results (Fig. 1(d)) indicate the correct judgment in structure of VOCl. And the structural parameters of the calculation show in Table S1. Figure 1(e) shows the identified three Raman modes at 93 K (see section 2 for Raman experimental parameters). The three peaks at around 200 cm^{-1}, 383 cm^{-1}, and 402 cm^{-1} can be assigned to A_g modes. These three modes are ascribed to the stretching vibrations of V–Cl bonds.[31] The absence of B_g modes might be the weak electron–phonon interactions.[32] The A_g and B_g are Raman-active phonons, see Subsection 3.2 for their specific meanings.

3.2. Angle-dependent polarized Raman spectra

Raman spectrum contains abundant information of crystal structural orientation and phonon vibration.[33] The Raman scattered intensity can be described as

$$I_S \propto \omega^4 |\boldsymbol{e}_i \cdot \overleftrightarrow{\boldsymbol{R}} \cdot \boldsymbol{e}_s|^2, \tag{1}$$

where ω is the angular frequency of the scattered light, $\boldsymbol{e}_i$ and $\boldsymbol{e}_s$ are the unit vector of the scattered and incident radiation, and $\overleftrightarrow{\boldsymbol{R}}$ is the second rank Raman tensor.[34] For the two-dimensional VOCl crystal, the non-vanishing polarizability tensor for the Raman active modes can be given by the following expression:

$$A_g \begin{pmatrix} a & 0 & 0 \\ 0 & b & 0 \\ 0 & 0 & c \end{pmatrix}, \quad B_g \begin{pmatrix} 0 & d & e \\ d & 0 & f \\ e & f & 0 \end{pmatrix}.$$

The incident laser parallels with the c axis of the crystal, which is polarized along the a axis or baxis of the crystal. In the laboratory frame XYZ, the Z axis coincides with the c axis. The Raman tensor can be described as

$$\begin{pmatrix} \cos\varphi & -\sin\varphi & 0 \\ \sin\varphi & \cos\varphi & 0 \\ 0 & 0 & 1 \end{pmatrix}^{-1} \begin{pmatrix} \alpha_{xx} & \alpha_{xy} & \alpha_{xz} \\ \alpha_{yx} & \alpha_{yy} & \alpha_{yz} \\ \alpha_{zx} & \alpha_{zy} & \alpha_{zz} \end{pmatrix} \begin{pmatrix} \cos\varphi & -\sin\varphi & 0 \\ \sin\varphi & \cos\varphi & 0 \\ 0 & 0 & 1 \end{pmatrix}.$$

Table 1. Under parallel and vertical scattering geometries, the anisotropic Raman scattering intensity for two vibrational modes in layered VOCl sample.

Raman mode	Parallel ($\boldsymbol{e}_i \parallel \boldsymbol{e}_s$)	Vertical ($\boldsymbol{e}_i \perp \boldsymbol{e}_s$)
A_g	$\lvert a\cos^2\theta + c\sin^2\theta\rvert^2$	$\lvert b\sin\theta\cos\theta - a\sin\theta\cos\theta\rvert^2$
B_g	$\lvert d\sin 2\theta\rvert^2$	$\lvert d\cos 2\theta\rvert^2$

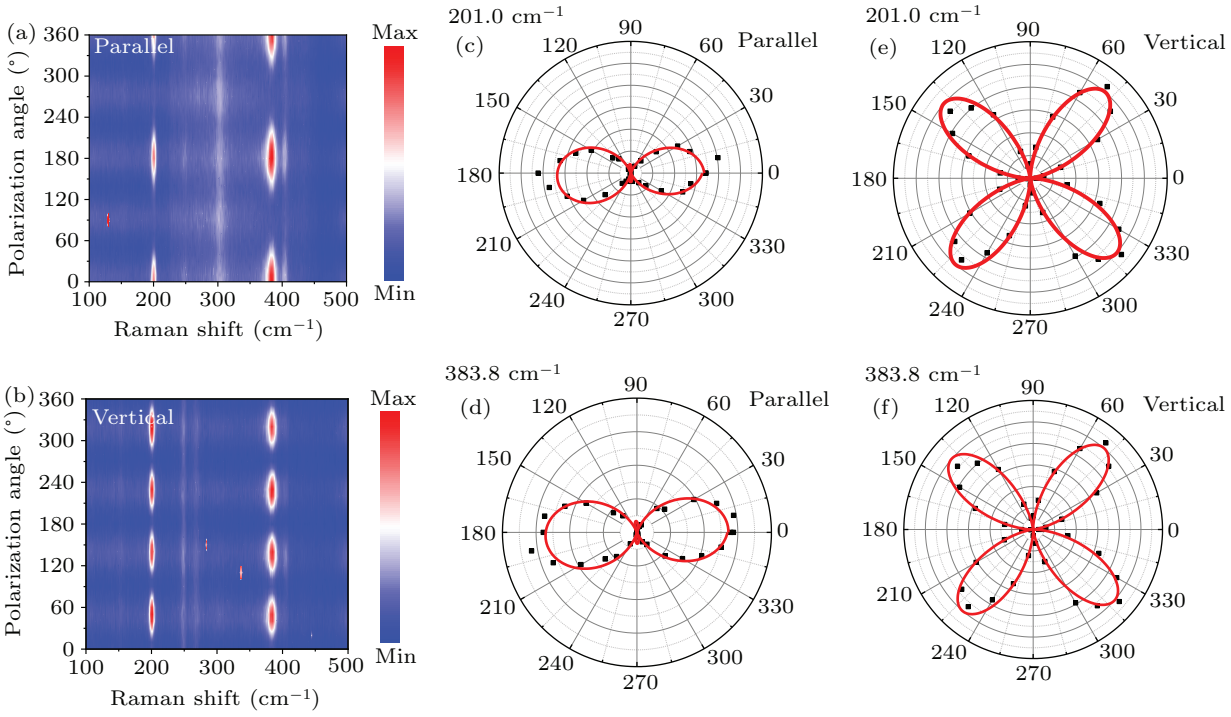


Fig. 2. The angle-resolved Raman spectroscopy of VOCl. (a) The contour colour map of Raman intensities under the parallel configuration. (b) The contour colour map of Raman intensities under the vertical configuration. (c)–(f) Polar plots of the Raman intensity change with respect to rotation angle.

The intermediate matrix is the Raman tensor of VOCl crystal, which is correspond to the A_g and B_g. In the laboratory frame, the Raman tensor elements can be given by

$$\begin{aligned}\alpha_{XX} &= \alpha_{xx}\cos^2\varphi + 2\alpha_{xx}\sin\varphi\cos\varphi + \alpha_{yy}\sin^2\varphi,\\ \alpha_{XY} &= -\alpha_{xx}\sin\varphi\cos\varphi + \alpha_{xy}(\cos^2\varphi - \sin^2\varphi)\\ &\quad + \alpha_{yy}\sin\varphi\cos\varphi.\end{aligned}$$

The Raman peak intensity in the parallel scattering geometry is $I_S \propto |\alpha_{XX}|^2$, and the Raman peak intensity in the vertical scattering geometry is $I_S \propto |\alpha_{XY}|^2$. Accordingly, the relationship between Raman peak intensity and angle for A_g and B_g modes under parallel and vertical polarizations is listed in Table 1.

To verify the above calculation results, the angle-resolved Raman spectroscopy experiments were carried out by rotating VOCl samples, and the results are shown in Fig. 2. It can be seen from Figs. 2(a) and 2(b) that the contour colour map of Raman intensities with rotation angles changing from 0° to 360° at a step of 10°. Under the parallel configuration, A_g^1 and A_g^2 modes have two maxima values at 0° and 180°. The intensity of A_g^3 is too weak to be distinguished, but the evolution period of A_g^3 is same as those of A_g^1 and A_g^2 modes. Under vertical configuration, A_g^1 and A_g^2 modes have four maxima values at 45°, 135°, 225°, and 315°, respectively. The evolution periods of A_g^1 and A_g^2 modes are $\pi/2$. Besides, figures 2(c)–2(f) shows the polar plots of A_g^1 and A_g^2 modes Raman position in parallel and perpendicular polarization configuration, in which the black dots are experimental values and the red lines represent the fitting result based on the above equations. A_g^1 and A_g^2 peaks show a 2-lobed shape in parallel polarization configuration but a 4-lobed shape in vertical configuration. This is consistent with the calculation in Table 1. The above results indicate that the polarized Raman intensities of VOCl are dependent on the crystal structural orientation.

3.3. Temperature-dependent Raman spectra

In addition, temperature-dependent Raman spectroscopy is highly important for further research of lattice vibration behavior. The contour colour map of low layer VOCl is shown in Fig. 3(a). Three modes peaks A_g^1, A_g^2, and A_g^3 can be distinguished. The temperature ranges of the experiment are from 93 K to 453 K with a step of 30 K. With the increase of temperature, the intensity of the Raman peak weakens obviously, which is probably because the anharmonic coupling of A_g modes are enhanced and Raman activity of the vibratory group is limited.[33] In addition to Raman peak intensity, the shift of the Raman peak position also contains a lot of information. To observe the shift of the Raman peak, figure 3(b) shows the enlarged view of offset in the A_g^1–A_g^3 peaks at different temperatures. It can be clearly seen that all three peaks show red-shift with the temperature going up, which is similar to experimental results from TMDs.[35–37] This shift is usually caused by electron–phonon, anharmonic phonon–phonon interaction and thermal expansion.[38,39]

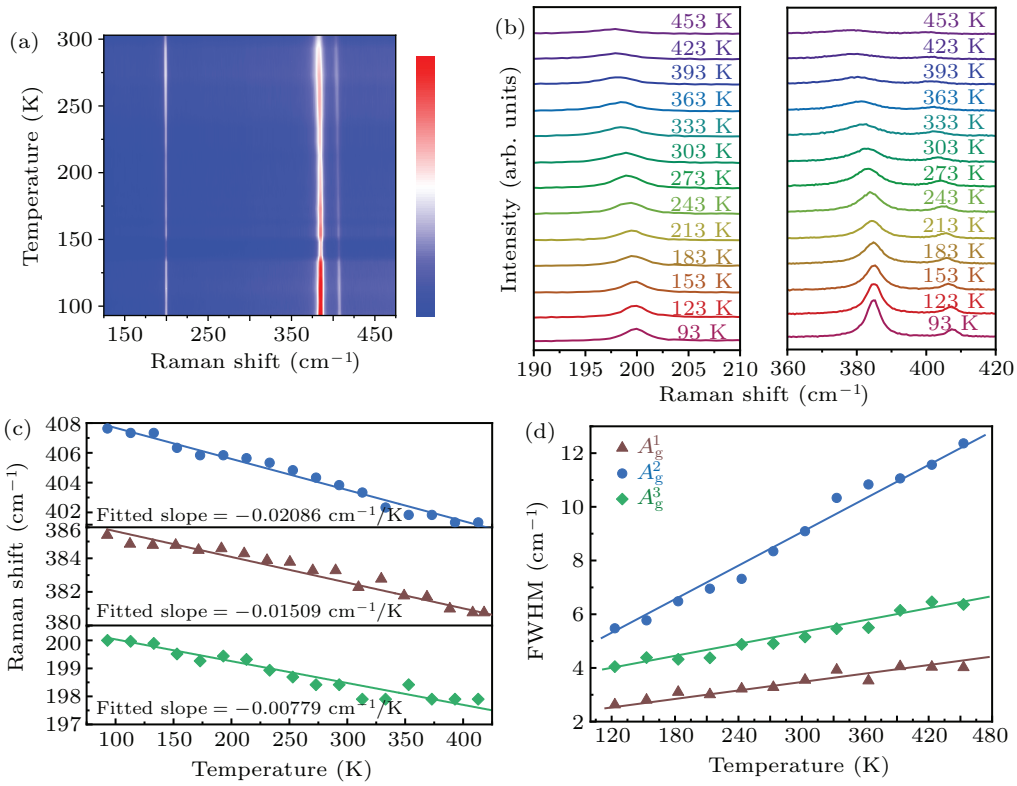


Fig. 3. Temperature-dependent Raman spectra of VOCl sample. (a) The contour colour map of temperature-dependent Raman spectra. (b) The typical modes for Raman peak positions as a function of temperature. (c) The first-order temperature coefficient fitting of Raman peaks. (d) The temperature-dependent FWHM of A_g^1, A_g^2, and A_g^3 modes for the Raman peaks of 2D VOCl.

The temperature-dependence of A_g^1, A_g^2, and A_g^3 phonon frequencies are linear, which can be fitted below:

$$\omega(T) = \omega_0 + \chi T,$$

where ω_0 is the phonon frequency of vibration modes at zero Kelvin temperature, and χ is the first-order temperature coefficient, which can be obtained from the slope of the fitted straight line. As shown in Fig. 3(c), the fitted first-order temperature coefficient χ for A_g^1, A_g^2, and A_g^3 modes are estimated as -0.00779, -0.01509, and -0.02086 cm^{-1}/K, respectively. It is indicated that A_g^3 modes are more sensitive to temperature. Moreover, the first-order temperature coefficient is proportional to the interlayer forces. The reported temperature coefficients of common two-dimensional materials are sorted out in Table S2.[38,40,41] Inferring that the interlayer forces of VOCl are similar to the TMDs system. This conclusion was also supported by the subsequent VOCl stripping process.

Meanwhile, the temperature-dependent full width at half maximum (FWHM) of A_g^1, A_g^2, and A_g^3 modes were examined as shown in Fig. 3(d). The broadening of phonon modes in Raman spectroscopy is the result of an optical phonon decaying into two distinct phonons caused by anharmonic forces in the crystal. Thus, the phonon lifetime is inversely proportional to the FWHM of the Raman peak.[42] With the increase of temperature, the FWHM of vibration modes increase linearly, indicating that the phonon lifetime (phonon relaxation time) decreases with the increasing temperature.[43]

3.4. Thickness-dependent optical properties

When the crystal has strong interlayer forces, thickness reduction also modulates the electron–phonon interaction, which appears as different vibrational bands in Raman spectra.[44] In order to investigate the interlayer forces of VOCl crystal. We conducted Raman test on VOCl with different thicknesses. The atomic force microscope (AFM) tests in Fig. 4(a) show that 2D VOCl flakes with thickness of 1.9 nm (two layer), 4.7 nm (five layer), 9.3 nm (ten layer), and 18.6 nm (twenty layer) were successfully exfoliated on 300-nm SiO_2/Si. The optical images of VOCl single crystal with different thicknesses are shown in Fig. S2. The corresponding Raman spectra of VOCl flakes with different thicknesses are shown in Fig. 4(b). This can be seen by contrast with bulk crystal, the vibration frequencies of A_g^1 (201.0 cm^{-1}), A_g^2 (383.8 cm^{-1}), and A_g^3 (402.9 cm^1) do not change with the thickness of VOCl flakes, indicating the interlayer van der Waal interaction in VOCl crystal is weak.

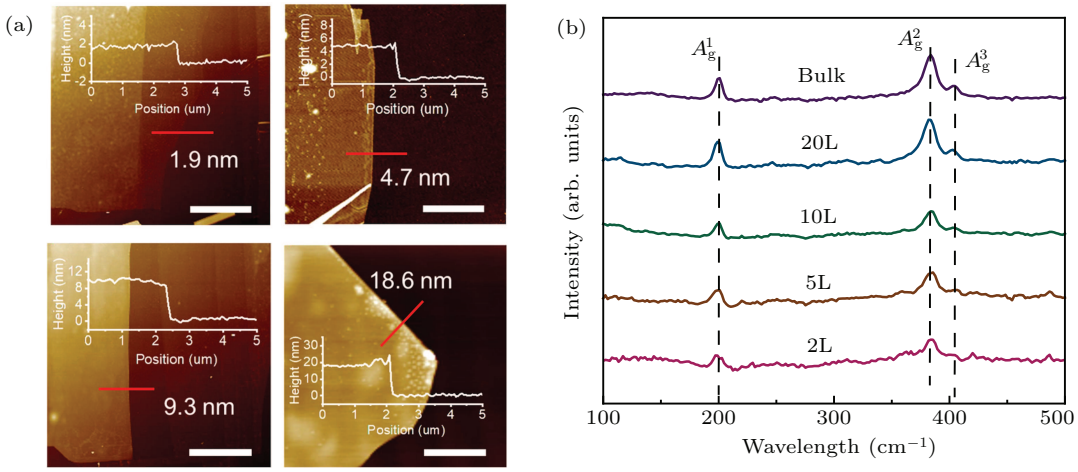


Fig. 4. (a) AFM images and corresponding curve of cross profiles of different VOCl samples, scale bar: 5 nm. (b) The Raman spectra of VOCl with several thicknesses.

4. Conclusions

In summary, we have successfully prepared 2D VOCl crystal and investigated its crystal structure and in-plane photon anisotropy. Employing the angle-dependent polarization Raman scattering experiment, the Raman peaks (A_g^1, A_g^2, and A_g^3) which belong to A_g vibrational modes are determined, and the specific shape shown in polar plots of the Raman intensity change with respect to rotation angle is consistent with the calculation. The temperature co-efficient for A_g^1, A_g^2, and A_g^3 modes were estimated as -0.00779 cm^{-1}/K, -0.01509 cm^{-1}/K, and -0.02086 cm^{-1}/K, respectively. The FWHM of different Raman modes in VOCl is observed to increase with temperature. Finally, the Raman spectra of 2D VOCl layers with different thicknesses are presented, three Raman peaks show little shift with thickness changes, proving the weak van der Waals force exists between layers of VOCl crystals. Based on the above experiments, this study could provide useful information for accelerating specific applications of 2D materials in the field of electronics and optics.

Acknowledgements

Project financially supported by National Natural Science Foundation of China (Grant No. U1932201), the International Partnership Program (Grant No. 211134KYSB20190063), the

CAS (Chinese Academy of Sciences) Collaborative Innovation Program of Hefei Science Center (Grant No. 2020HSC-CIP002), the University Synergy Innovation Program of Anhui Province, China (Grant No. GXXT-2020-002), the Youth Innovation Promotion Association of CAS (Grant No. 2022457), and the USTC Research Funds of the Double First-Class Initiative (YD2310002004).

We thank the Shanghai Synchrotron Radiation Facility (14W1 and 14B1, SSRF), the Beijing Synchrotron Radiation Facility (1W1B, 4W1B, and 4B9A, BSRF), the Hefei Synchrotron Radiation Facility (MCD-A and MCD-B Soochow Beamline for Energy Materials, Catalysis/Surface Science Endstations at NSRL), and the USTC Center for Micro and Nanoscale Research and Fabrication for helps in characterizations.

References

[1] Ling X, Wang H, Huang S, Xia F and Dresselhaus M S 2015 *Proc. Natl. Acad. Sci. USA* **112** 4523
[2] Xiaomu W, Aaron MJ, Kyle LS, Vy T, Yichen J, Huan Z, *et al.* 2015 *Nat. Nanotechnol.* **10** 517
[3] Xia F, Wang H and Jia Y 2014 *Nat. Commun.* **5** 4458
[4] Fang Y, Pan J, He J, Luo R, Wang D, Che X, *et al.* 2018 *Angew. Chem. Int. Ed.* **57** 1232
[5] Nam G H, He Q, Wang X, Yu Y, Chen J, Zhang K, *et al.* 2019 *Adv. Mater.* **31** 1807764
[6] Chenet D A, Aslan O B, Huang P Y, Fan C, van der Zande A M, Heinz T F, *et al.* 2015 *Nano Lett.* **15** 5667
[7] Liu F, Zheng S, He X, Chaturvedi A, He J, Chow W L, *et al.* 2016 *Adv. Funct. Mater.* **26** 1169
[8] Zhang E, Wang P, Li Z, Wang H, Song C, Huang C, *et al.* 2016 *ACS Nano* **10** 8067
[9] MacNeill D, Stiehl G M, Guimaraes M H D, Buhrman R A, Park J and Ralph D C 2017 *Nat. Phys.* **13** 300
[10] Song Q, Pan X, Wang H, Zhang K, Tan Q, Li P, *et al.* 2016 *Sci. Rep.* **6** 29254
[11] Huang S, Tatsumi Y, Ling X, Guo H, Wang Z, Watson G, *et al.* 2016 *ACS Nano* **10** 8964
[12] Yang S, Liu Y, Wu M, Zhao L D, Lin Z, Cheng H C, *et al.* 2018 *Nano Res.* **11** 554
[13] Zhang C, Ouyang H, Miao R, Sui Y, Hao H, Tang Y, *et al.* 2019 *Adv. Opt. Mater.* **7** 1900631
[14] Papadakis S J, De Poortere E P, Shayegan M and Winkler R 2000 *Phys. Rev. Lett.* **84** 5592
[15] Cui Q, Luo Z, Cui Q, Zhu W, Shou H, Wu C, *et al.* 2021 *Adv. Funct. Mater.* **31** 2105339
[16] Guo J, Liu Y, Ma Y, Zhu E, Lee S, Lu Z, *et al.* 2018 *Adv. Mater.* **30** 1705934
[17] Zhou Z, Cui Y, Tan P H, Liu X and Wei Z 2019 *J. Semicond.* **40** 061001
[18] Glawion S, Scholz M R, Zhang Y Z, Valentí R, Saha-Dasgupta T, Klemm M, *et al.* 2009 *Phys. Rev. B* **80** 155119
[19] Schönleber A, Angelkort J, van Smaalen S, Palatinus L, Senyshyn A and Morgenroth W 2009 *Phys. Rev. B* **80** 064426
[20] Zhu W, Cui Q, Adam M L, Liu Z, Zhang L, Dai Z, *et al.* 2021 *2D Mater.* **8** 025010
[21] Wang W J, Xu X T, Shen J, Wang Z, Zhang S L and Qu Z 2021 *Chin. Phys. B* **30** 107502
[22] Miao N, Xu B, Zhu L, Zhou J and Sun Z 2018 *J. Am. Chem. Soc.* **140** 2417
[23] Yao Y, Zhang Y, Xiong W, Wang Z, Sendeku M G, Li N, *et al.* 2019 *Adv. Funct. Mater.* **29** 1903017
[24] Zhang X, Qiao X F, Shi W, Wu J B, Jiang D S and Tan P H 2015 *Chem. Soc. Rev.* **44** 2757
[25] Late D J, Liu B, Matte H S S R, Rao C N R and Dravid V P 2012 *Adv. Funct. Mater.* **22** 1894
[26] Wang X, Shi W, She G and Mu L 2011 *J. Am. Chem. Soc.* **133** 16518
[27] Wu J, Mao N, Xie L, Xu H and Zhang J 2015 *Angew. Chem. Int. Ed.* **54** 2366
[28] Lu D, Luo S, Liu S, Yao H, Ren X, Zhou W, *et al.* 2018 *J. Phys. Chem. C* **122** 24459
[29] Luo S, Qi X, Yao H, Ren X, Chen Q and Zhong J 2017 *J. Phys. Chem. C* **121** 4674
[30] Tongay S, Sahin H, Ko C, Luce A, Fan W, Liu K, *et al.* 2014 *Nat. Commun.* **5** 3252
[31] Ping Gao, *et al.* 2016 *J. Electrochem. Soc.* **163** A2326
[32] Zhang T, Wang Y, Li H, Zhong F, Shi J, Wu M, *et al.* 2019 *ACS Nano* **13** 11353
[33] Fang Y, Wang F, Wang R, Zhai T and Huang F 2021 *Adv. Mater.* **33** 2101505
[34] Chen H, Li Y, Wu H, Peng Y, Fang Y, Chen C, *et al.* 2019 *Solid State Commun.* **289** 56
[35] Viana B C, Alencar R S, Vieira A G, Carozo V, Filho A G S, Wang J, *et al.* 2020 *Vib. Spectrosc.* **111** 103169
[36] Chen Y, Deng C, Wei Y, Liu J, Su Y, Xie S, *et al.* 2021 *Appl. Phys. Lett.* **119** 063104
[37] Sahoo S, Gaur A P S, Ahmadi M, Guinel M J F and Katiyar R S 2013 *J. Phys. Chem. C* **117** 9042
[38] Late D J, Maitra U, Panchakarla L S, Waghmare U V and Rao C N R 2011 *J. Phys.: Condens. Matter* **23** 055303
[39] Taube A, Judek J, Jastrzębski C, Duzynska A, Świtkowski K and Zdrojek M 2014 *ACS Appl. Mater. Interfaces* **6** 8959
[40] Pawbake A S, Pawar M S, Jadkar S R and Late D J 2016 *Nanoscale* **8** 3008
[41] Luo Z, Maassen J, Deng Y, Du Y, Garrelts R P, Lundstrom M S, *et al.* 2015 *Nat. Commun.* **6** 8572
[42] Li Z, Wang Y, Jiang J, Liang Y, Zhong B, Zhang H, *et al.* 2020 *Nano Res.* **13** 591
[43] Irfan B, Sahoo S, Gaur A P S, Ahmadi M, Guinel M J F, Katiyar R S, *et al.* 2014 *J. Appl. Phys.* **115** 173506
[44] Lee S, Kim K, Dhakal K P, Kim H, Yun W S, Lee J, *et al.* 2017 *Nano Lett.* **17** 7744